

Fine Structure Recognition in Multichannel Observations

Stanislava Šimberová

Astronomical Institute, Academy of Sciences
Ondřejov, CZ251 65, Czech Republic
Email: ssimbero@asu.cas.cz

Michal Haindl

and Filip Šroubek
Institute of Information Theory and Automation
Academy of Sciences
Prague 8, CZ182 08, Czech Republic
Email: haindl, sroubekf@utia.cas.cz

Abstract—Two restoration methods applied to the multitemporal solar images are presented. Our main goal is to model and remove degradation in a subimage, where a specific event is investigated. Using information of the input (blurred) channels within a short observed sequence a new undegraded image is reconstructed. Degradation is assumed to follow a linear degradation model with an unknown possibly non-homogeneous point spread function (PSF) and additive noise. The first method (VAM) is based on multichannel blind deconvolution (MBD) using a variational approach to blur estimation, while the second one (SAM) supposes solution of the multidimensional causal regressive model representing the degraded image (channel). Experimental image data are from the ground based observation (white light) and satellite SOHO mission - EIT (EUV). Contributions of both suggested methods and their generalization are discussed.

I. INTRODUCTION

It is common knowledge, that the image degradation is caused by random fluctuations of the optical way between the object space and the image formation space. As to the ground-based observations in visible light, the image quality in the image space decreases by variations of the index of refraction, dominated by the thermal turbulence. Influence of the turbulence in image formation were analyzed since the 1950s, see e.g. [1], [2], [3]. In a simplified fashion all these negative influences of image formation process can be involved into the changing complex point spread function (PSF) with various value of importance. The more precise mathematical description of observing conditions leads to a better determination of constraints providing improvement of the solution stability. Image data coming from space observations (Missions SOHO, TRACE, HINODE, SDO, etc.) do not suffer from the atmospheric turbulences, but can be degraded by other disturbing sources. In particular the thermal effects in mechanical and optical parts cause degradations revealing in defocusation, distortion, blur motion, etc. All these influences can cause serious damage or data loss. Completing the multiwavelength data sets requires restoration of details. As to the solar image data, typical example is e.g. small area of an active region within the whole disc (satellite data of SOHO - EIT, MDI, etc.). Another one is the sector of sunspot penumbra in the white light observation or details of the flare in H α line, etc.

From the restoration point of view we consider a general degradation model, i.e. there is only one degradation complex unknown function involving all aspects of degradation. The degradation function model has to differentiate among different types of astronomical observations. There are obviously distinct assumptions in modeling of degradation by the long-exposure stellar objects (exposure time of about minutes) and the short-exposure solar images (exposure time of about milliseconds).

Image reconstruction is unfortunately an ill-posed problem, [4]. Any application of a new method to the real data needs to find a set of astronomical images according to the constraints defined in the input of the algorithm.

Many different image restoration methods have been published and several sophisticated algorithms in the last 20 years have been applied. Most of these methods are general purpose image restoration algorithms which cannot benefit from the specific multitemporal observation measurement setup.

A thorough overview of reconstruction problem is described in [5], another review on image reconstruction in astronomy is given in [6] or [7].

The simplest restoration method is to smooth the data with an isotropic linear or non-linear shift-invariant low-pass filter. Usually these techniques tend to blur edges in images. Several methods, e.g. [8], try to avoid this problem by using a large number of low-pass filters and combining their outputs. Similarly anisotropic diffusion, see [9], [10] addresses this problem but it is computationally extremely demanding. Image intensity in this method is allowed to diffuse over time, with the amount of diffusion at a point being inversely proportional to the magnitude of local intensity gradient.

The methods of Tikhonov regularization, maximum entropy, and total variation (see e.g. [6], [7]) impose global image preference functions. The drawback of global methods overcome spatially adaptive methods, such as e.g. spatially variable entropy, wavelets, Markov random fields, Gibbs priors, etc.

Model-based methods use most often the Markov random field type of models either in the form of wide sense Markov (regressive models) or strong Markov models. The noncausal regressive model used in [11] has the main problem in time consuming iterative solution based on the conjugate gradient method. Similarly Markov random field based restoration

methods, e.g. [12], [13], [14], require time consuming application of Markov chain Monte Carlo methods.

As to the multichannel deconvolution approach, an overview of various methods for astronomical input data is given in [7].

Demands on the observed image data are completely different for the data obtained in various parts of the spectrum (from gamma, X, via visible, IR up to radio wavelength). The PSF varies with time or within the observed field. The observation is limited by the optical power of the telescope (diffraction limited) and by the atmospheric effects (seeing limited). The atmospheric turbulence produces images with seeing limited spatial resolution during the ground-based observation in the visible and near IR range of spectrum. This effect is much lower than the theoretical diffraction limit. Technically speaking there are two methods for restoration of this solar image category: speckle interferometry and phase diversity. Their applications need a special observational mode and appropriate hardware support. For this reason the methods are not applicable to image data obtained in common observational mode. Principles, conditions, and some examples are given in [15].

Our approach to the image restoration differs from direct and indirect techniques like various types of filtering, power spectra equalization, constrained least-squares restoration, maximum entropy restoration, etc. We do not assume any prior knowledge about the degradation process and furthermore our solution is analytical and fast. The image restoration task is to recover an unobservable (ideal) image given the short sequence differently corrupted images with respect to some statistical criterion.

We introduce two restoration algorithms: The VAM method, based on principle of blind deconvolution in the Bayesian framework. The second one is SAM, modeling the corruption process by the multidimensional causal regressive model.

The next sections introduce two approaches of image restoration based on modification of the multichannel deconvolution using Bayesian methodology and the spatially adaptive image restriction method. The follow-up section covers theoretical background, continuing experimental part with simulations and results with the real data. In discussion we try to evaluate both solutions and to compare presumptions and advantages of the methods.

II. MULTIPLE INPUT CHANNEL METHODS

Due to a short sequence observation setup we can legitimately assume that all observed degraded images are mutually ideally registered, they contain identical scene and their degradations differ for every observation. An example of the real short-exposure image of solar photosphere is in Fig.1.

The image degradation is supposed to be approximated by the linear discrete spatial domain degradation model

$$X_{r,\bullet} = \sum_{s \in I_r} H_{s,\bullet} Y_{r-s} + \nu_{r,\bullet}, \quad (1)$$

where $H_{s,\bullet}$ is the $d \times 1$ vector of the s-th pixel in different unknown PSFs, $X_{r,\bullet}$ is the $d \times 1$ vector of the r-th pixel in different distortions and Y_\bullet are ideal (unobservable) image

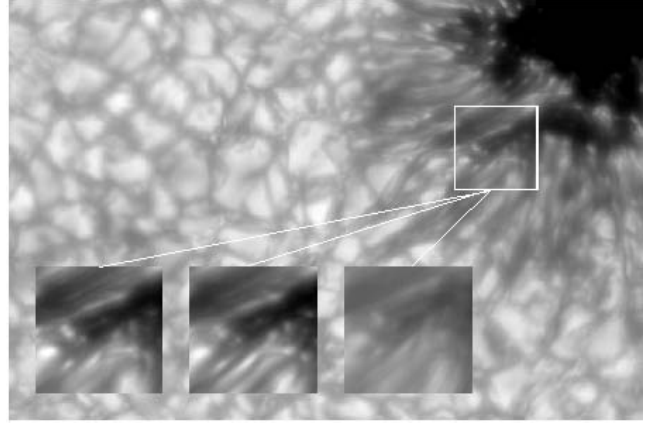


Fig. 1. The high resolution image with framed detail. The zoomed random samples of channels 11, 19, 24 from left to right. Data origin: telescope 1-m SST, La Palma, 2004-06-15, observer M. Sobotka.

pixels. The number of observed images is d . I_r is some contextual support set, and a noise vector ν is uncorrelated with the true image.

A. Variational Method (VAM)

This approach is based on the work of Amizic *et al.* [16] for multichannel blind deconvolution in the Bayesian framework. Simultaneous autoregression was used for the image prior distribution:

$$p(Y) \approx \exp \left\{ -\frac{1}{2} \alpha \|\Delta Y\|^2 \right\}, \quad (2)$$

where Δ denotes the Laplacian operator and α is the inverse variance of Gaussian distributions. This prior models accurately the nature of studied images.

From the observation model (1) and assumption that noise ν is Gaussian with zero mean and variance equal to β^{-1} , we obtain

$$p_1(X|Y, H) \approx \exp \left\{ -\frac{1}{2} \beta \sum_i \sum_r (X_{r,i} - \sum_{s \in I_r} H_{s,i} Y_{r-s})^2 \right\}. \quad (3)$$

The multichannel case allows us to formulate additional observation model as we proposed in [17]:

$$p_2(X|H) \approx \exp \left\{ -\frac{1}{2} \gamma \sum_{1 \leq i < j \leq d} \sum_r \left(\sum_{s \in I_r} H_{s,i} X_{r-s,j} - \sum_{s \in I_r} H_{s,j} X_{r-s,i} \right)^2 \right\}. \quad (4)$$

We use logarithmic opinion pooling technique to combine both observation models and get

$$p(X|Y, H) \approx p_1(X|Y, H)^{\lambda_1} p_2(X|H)^{\lambda_2}, \quad (5)$$

where $\lambda_1 + \lambda_2 = 1$ and $\lambda_1, \lambda_2 \geq 0$.

Following the Bayesian paradigm, the posterior distribution takes the form

$$p(Y, H|X) = p(X|Y, H)p(Y)p(H)/p(X), \quad (6)$$

where for the prior $p(H)$ a non-informative uniform distribution was chosen.

Using the Kullback-Leibler (C_{KL}) divergence, we then approximate the posterior distribution of the unknown image and PSFs by a product $q(Y)q(H)$, where $q(Y)$ denotes a distribution on the true image Y and $q(H)$ denotes a degenerate distribution on PSFs. Alternating minimization of C_{KL} with respect to $q(Y)$ and $q(H)$ leads to an iterative algorithm:

$$q^k(Y) = \arg \min_{q(Y)} C_{KL}\{q(Y)q^k(H)\|p(Y, H|X)\} \quad (7)$$

$$q^{k+1}(H) = \arg \min_{q(H)} C_{KL}\{q^k(Y)q(H)\|p(Y, H|X)\} \quad (8)$$

As an estimate of the true image we take $E\{Y\}_{q^k(Y)}$ at the step k , when a convergence criterion is met.

B. Spatially Adaptive Method (SAM)

This method generalizes our monospectral restoration ([18]) for the multiversion images. The term "multiversion" is used in the sense of multichannel input where each channel represents one image out of a short time sequence.

According to the processing methods classification [5], it is possible to assign our method to the class of techniques, which can adapt themselves to different image conditions.

A similar combination of causal and non-causal regressive models as in this paper was used in [19]. However they assume the homogeneous point-spread function and they identify all parameters simultaneously using extremely time consuming iterations of the EM (expectation maximization) algorithm which is not guaranteed to reach the global optimum.

In (1) a global point-spread function is assumed to be either homogeneous or it can be non-homogeneous but in this case we assume the PSF changes slowly relative to the size of an image. It is unknown but such that we can assume the unobservable image Y to be reasonably well approximated by the expectation of the corrupted image

$$\hat{Y} = E\{X_{\bullet,i}\} \quad (9)$$

in regions with gradual pixel value changes, and the i -th degraded image $X_{\bullet,i} \in \mathcal{X}$ is the least degraded image from the set \mathcal{X} . The SAM method changes pixels during the restoration process and thus might blur discontinuities present in the scene but to much less extent than the classical restoration methods due to our restoration model adaptivity and adaptive restoration switching (10).

This excessive blurring can be avoided if pixels with steep step discontinuities are left unrestored, i.e.

$$\hat{Y}_r = \begin{cases} E\{X_r\} & \text{if } p(X_r | X^{(r-1)}) > \kappa \\ X_r & \text{otherwise} \end{cases}, \quad (10)$$

where κ is a probabilistic threshold based on the prediction density. Single matrix elements in the expectation $E\{X\}$ are approximated [20] by the conditional expectation $E\{X_j | X^{(j-1)}\} = x^{(j-1)}$ where $x^{(j-1)}$ are known past

realization for j . Thus we suppose that all other possible realization $x^{(j-1)}$ than the true past pixel values have negligible probabilities. This assumption implies conditional expectations approximately equal to unconditional ones, i.e., then the expectation is $E\{X_j\} \approx E\{X_j | X^{(j-1)}\}$.

Suppose further that a noisy image can be represented by an adaptive 2.5D causal simultaneous autoregressive model

$$X_{r,i} = \sum_{s \in I_r^c} A_s X_{r-s,\bullet} + \epsilon_r, \quad (11)$$

where ϵ_r is a white Gaussian noise vector with zero mean. $A_s = [a_{s,1}, \dots, a_{s,d}] \forall s$ are parameter vectors. Any image can be locally represented by this adaptive linear model when its parameters are estimated from the observed data. The noise vector is uncorrelated with data from a causal neighborhood I_r^c . The model adaptivity is introduced using the exponential forgetting factor technique in parameter learning part of the algorithm. The conditional mean value $E\{X_r | X^{(r-1)}\}$ can be derived under few acceptable conditions and an appropriate model support (I_r^c) can be found using the Bayesian decision rule. The detail mathematical deduction is in [20].

III. DATA SIMULATIONS

In order to illustrate that the proposed VAM algorithm performs multichannel blind deconvolution of astronomical data blurred by Gaussian-like PSFs under different noise levels, we conducted an experiment on simulated data.

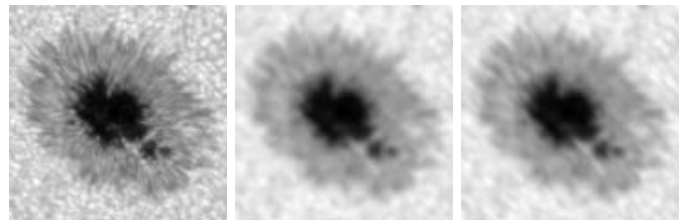


Fig. 2. Simulations: The "known" original image (left), artificially degraded to input1 (middle) and input2 (right).

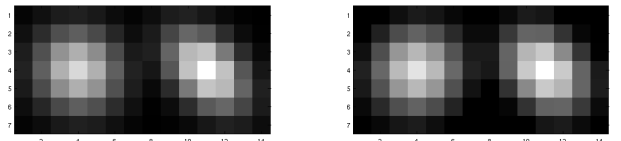


Fig. 3. The randomly generated PSFs used in input1 and input2 channels (left pair), and corresponding estimated PSFs using the VAM algorithm (right pair).

We took a real sun-spot image 128x128 in Fig. 2 left and degraded it by two random Gaussian blurs of size 7x7 and additive noise with SNRs 50, 40, 30 and 20 dB. Random means that the covariance matrix of the Gaussian function

was randomly generated, with diagonal variances between 1 and 3, see example in Fig. 3 left. For each SNR, 20 pairs of blurred images were generated and then deconvolved with VAM. An example of one such pair of blurred images with $\text{SNR} = 50 \text{ dB}$ is depicted in Fig. 4 (left and middle) and the corresponding VAM estimation of the sharp image (right). The estimated PSFs are in Fig. 3 right. One can see that the reconstructed PSFs match exactly the original PSFs and the reconstructed image closely resembles the original one. ISNR (Improved SNR) is defined as $10 \log \frac{\|\mathbf{Y} - \hat{\mathbf{Y}}\|^2}{\|\mathbf{Y} - \mathbf{X}\|^2}$, where $\hat{\mathbf{Y}}$ is the VAM estimation of the original image \mathbf{Y} mean and variance for each SNR over 20 reconstructions is given in Fig. 5. Naturally, ISNR decreases with the increasing noise level but the performance is stable as the ISNR variance is not very high.

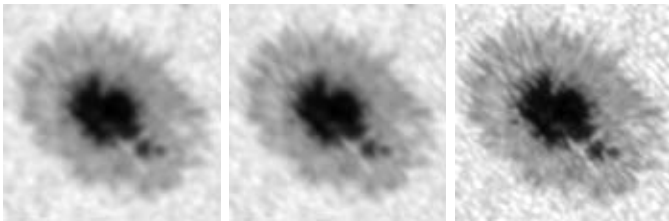


Fig. 4. Input channels input1 (left), input2 (middle), and reconstructed image (right) using the VAM algorithm.

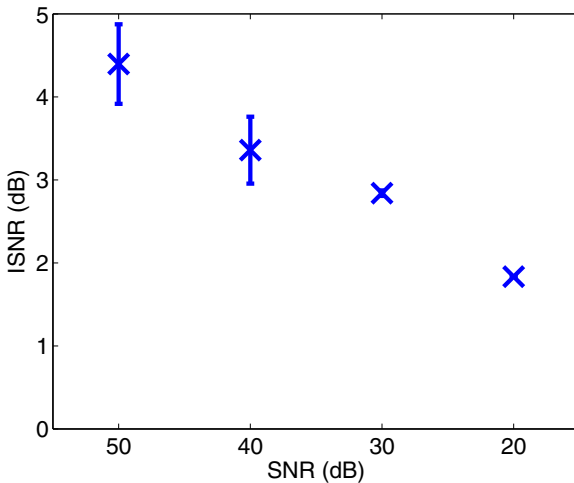


Fig. 5. Statistics in simulated experiments: The mean value and standard deviation of improved SNR (ISNR) in dependence of input data SNR.

IV. REAL DATA EXPERIMENTS

A. The ground-based observations

We used a sequence of image data observed in the visible range of spectrum. In Fig. 1 is one plane of the vision field of data cube record with framed subimages. These details represent input channels in time for the algorithm. Data

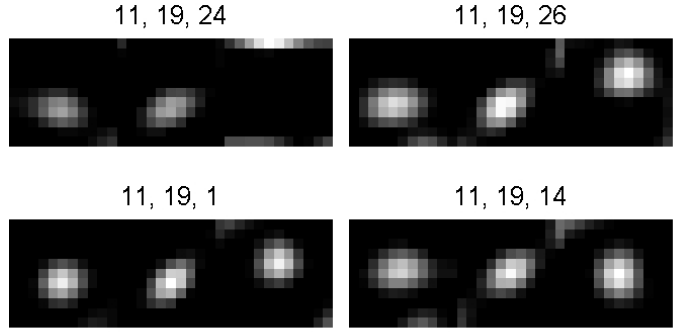


Fig. 6. The VAM: Estimated PSFs for different combinations of channels. The size and shape reflect the visual quality of the channel.

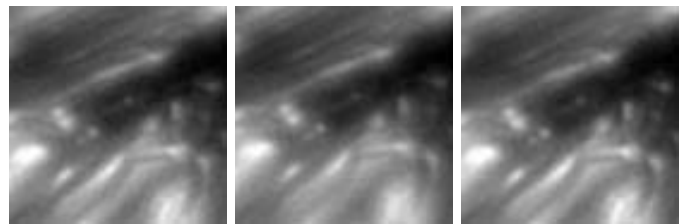


Fig. 7. Results of VAM: reconstructed from inputs 11, 19 (left); 11, 26 (middle); 11, 19, 14 (right).

specification: wavelength $\lambda = 4507.5 \text{ \AA}$, $\Delta\lambda = 9.2 \text{ \AA}$, $t_{exp} = 15 \text{ ms}$, estimated seeing (0.2 - 0.4) arcsec, flat field corrected, adaptive optics used. Time interval of the sequence is in $t \leq 5 \text{ s}$, i.e. cadence is 6 images per second. The original sampling is 1 pixel = 0.0405 arcsec (high resolution).

The channel Nr. 24 (right subimage in Fig. 1) was identified by preprocessing procedure during observation (rms value) as the worst one and was excluded from the input set of data. Afterward it was confirmed by the PSF estimation using the VAM algorithm, see the degenerative PSF of channel Nr. 24 in Fig. 6 (upper left, the third one in row).

Some results of VAM reconstruction from the two resp. three input channels are in Fig. 7. Different number and combinations of input images was tested for VAM reconstruction. The optimal reconstruction with no visible artifacts was obtained using three input images. If we use more than four inputs, the reconstructed PSFs are less compactly supported and the final image begins to exhibit artifacts. This observation is in accordance with conclusions drawn in [21]. In theory, the reconstruction process is better posed with an increasing number of input images. However, real data do not follow exactly the assumed model (1) and as discrepancies in the data grow stronger the reconstruction process deteriorates.

Reconstruction result using the SAM restoration is in Fig. 8 together with the corresponding prediction probability images. The gray level coded predictor probabilities served to control the restoration switching. The lighter shades represent higher predictor probabilities while dark areas were not changed during the reconstruction. In Fig. 9 are results of VAM and

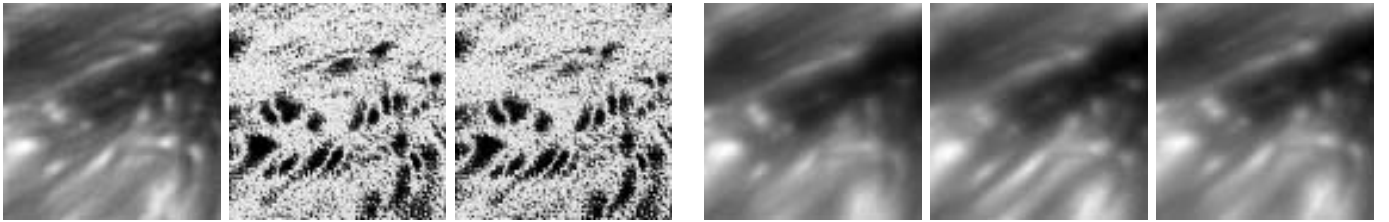


Fig. 8. Results of SAM: reconstructed from inputs 11,19 (left), and its corresponding prediction probability image (middle); for comparison the prediction probability image using three input channels 11, 19, 26 (right).

SAM while the same input channels were used.

B. The satellite observations

Another processed set of image data is from the SOHO mission, aboard device EIT (Extreme ultraviolet Image Telescope). Observed sequence efz20040825 (Aug.25, 2004), wavelength $\lambda = 195 \text{ \AA}$, 1 pixel = 2.6 arcsec. The satellite data are fortunately free from atmospheric degradation, but can be corrupted in various ways as was already mentioned. A serious degradation is so-called "spatial noise", mostly of indistinct origin. Especially in analysis of smallest events it is important to solve this problem even on the pixel and subpixel level. The detail description of solar EUV image degradation is in [22]. We can assume approximately constant level of noise for all channels. For our experiments the one-minute-cadence EIT sequence has been used. We extracted 9 successive images representing the input channels for both methods. The standard EIT image (full disc) with framed subimage is in Fig. 10, examples of input channels are in Fig. 11. In Fig. 12 there are some combinations of estimated PSFs and Fig. 13 shows the VAM and SAM reconstruction from three different combinations of channels.

Restoration quality for the SAM method was validated using several blind restoration criteria for solar images as well as for artificially simulated data, see [23] for details. According to these results (not presented here), the optimal restoration was performed by nine channels (Fig. 14). The second best restoration was evaluated from three channels 1, 2, 3 (see Fig. 13, bottom foursome, right from input No. 9).

V. CONCLUSIONS

We have developed two independent restoration methods **VAM** and **SAM** based on multichannel approach. The main goal is to model and remove degradation in the small areas of observed degraded images. Both algorithms were applied to solar images obtained from the ground-based observation (optical range) and satellite observation SOHO-EIT (EUV range). The methods were tested on synthetic data damaged by known degradation functions. We compared the result of reconstruction with the known original image. The estimated degradation functions are compared with the apriori known functions used in artificial blurring.

The real data restoration, where the "ideal" image is unknown, is based on recovering information of input blurred

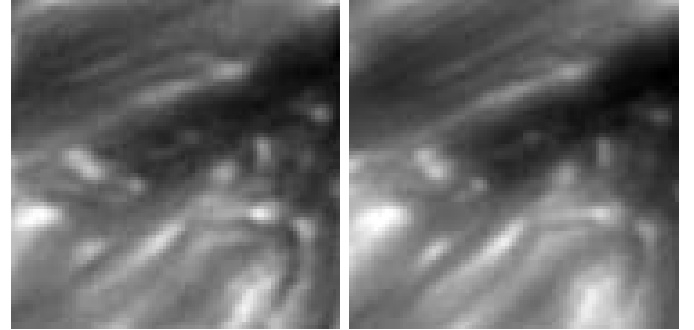


Fig. 9. Top row: Original input channels 11, 19 and 26. Bottom row: enlargement of reconstruction results SAM (left) and VAM (right) using the upper input channels.

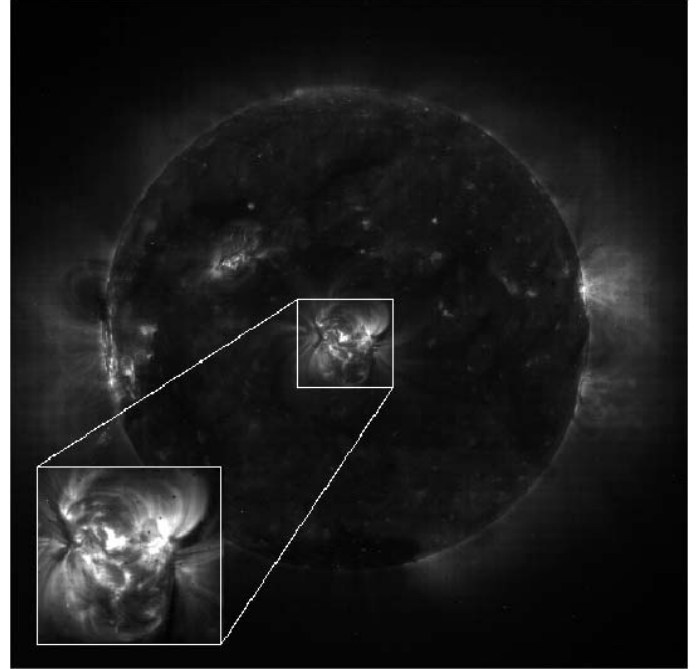


Fig. 10. The regular-size EIT image with the framed subimage.

channels. Simultaneously the degradation functions in each input channel are estimated.

VAM: We experimentally proved that this method performs well in the case of images blurred by unknown blurs and corrupted by noise, which renders the method to be stable in blind deconvolution of real astronomical data if at least two blurry images of the same object are provided. On the basis of a PSF estimation (size, shape, homogeneity) the

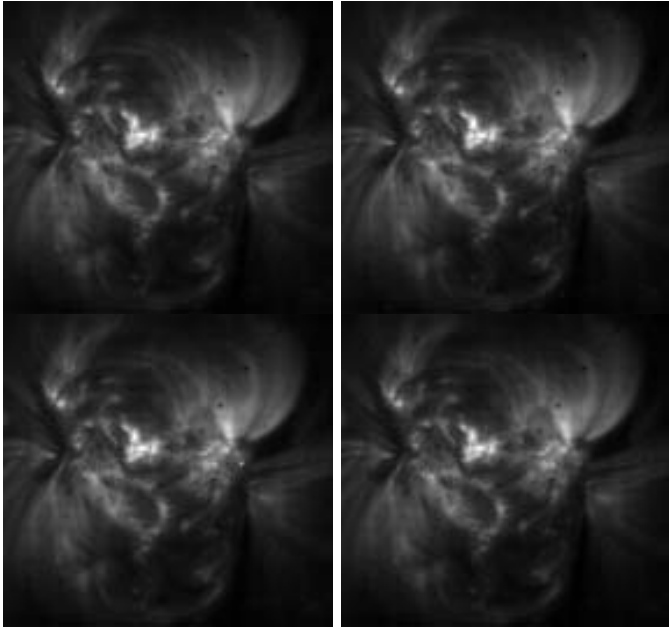


Fig. 11. Examples of channel inputs - EIT data (from left upper to right bottom inputs 1, 4, 7, 9).

VAM determines the worst degraded channel(s), which is(are) instantaneously excluded from the reconstruction process.

SAM: Our previous results of experiments in [20] were confirmed here, the method performs reconstruction based on information of the best input channels. Causal models have obvious advantage in the fast analytical solution for parameter estimation, prediction, or model identification. The SAM is extremely fast and numerically stable and can be easily advantageously applied to bulky restoration tasks (large frame resolution, numerous channels, etc.). Possible undesirable effects (causality artifacts) are diminished by introducing the adaptivity into the model. This novel formulation permits us to obtain extremely fast adaptive multichannel restoration and it can be easily parallelized due to the restoration model causality. Finally this method enables to estimate homogeneous or slowly changing nonhomogeneous PSF. The SAM's by-product, the prediction probability map (Fig. 14 upper left), can significantly contribute to a design of novel superresolution methods.

For the future we intend to compare the VAM and SAM performance in dependence of optimal number of input channels, and to follow the stability of solution for increasing field of view.

ACKNOWLEDGMENT

We say thank Vincent Barra for sharing of fast-cadence EIT data. This research was supported by the projects no. GAČR 102/08/1593, GAČR 102/08/0593, GAČR P103/11/1552 and partially by the grant CESNET 409/2011.

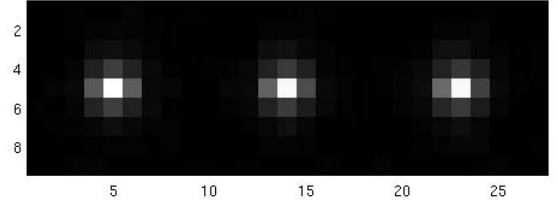
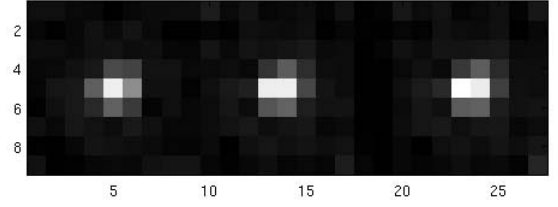


Fig. 12. EIT data: Estimated PSFs for input channel combinations: 1, 2, 3 (upper), 4, 5, 6 (bottom).

REFERENCES

- [1] D. Fried, "Optical resolution through a randomly inhomogeneous medium for very long and very short exposures," *J. Opt. Soc. Am.*, vol. 56, p. 1372, 1966.
- [2] F. Roddier, in *Progress in Optics*, E. Wolf, Ed., vol. XIX. Amsterdam: Nort-Holland, 1981, p. 281.
- [3] T. Schulz, "Multiframe blind deconvolution of astronomical images," *J. Opt. Soc. Am. A*, vol. 10, no. 5, pp. 1064–1073, 1993.
- [4] J. C. Russ, *The image processing handbook*. Boca Raton: CRC Press, Inc., 1995.
- [5] R. C. Puetter, T. R. Gosnell, and A. Yahil, "Digital image reconstruction: Deblurring and denoising," *Ann. Rev. Astrophys.*, vol. 43, pp. 5.1–5.56, 2005.
- [6] R. Molina, J. Núñez, F. J. Cortijo, and J. Mateos, "Image restoration in astronomy: A bayesian perspective," *IEEE Signal Processing Magazine*, no. 3, pp. 11–29, March 2001.
- [7] J. L. Starck, E. Pantin, and F. Murtagh, "Deconvolution in astronomy: A review," *Publ. Astr. Soc. Pac.*, vol. 114, pp. 1051–1069, 2002.
- [8] P. Perona, "Deformable kernels for early vision," *IEEE Trans. Pattern Anal. Mach. Int.*, vol. 17, no. 5, pp. 488–489, May 1995.
- [9] P. Perona and J. Malik, "Scale-space and edge detection using anisotropic diffusion," *IEEE Trans. Pattern Anal. Mach. Int.*, vol. 12, no. 7, pp. 629–639, July 1990.
- [10] B. Fischl and E. Schwartz, "Learning an integral equation approximation to nonlinear anisotropic diffusion in image processing," *IEEE Trans. Pattern Anal. Mach. Int.*, vol. 19, no. 4, pp. 342–352, April 1997.

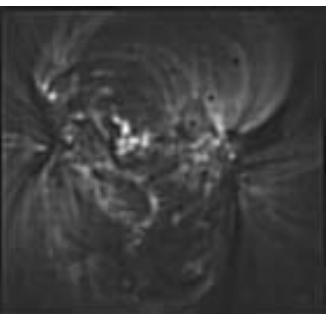
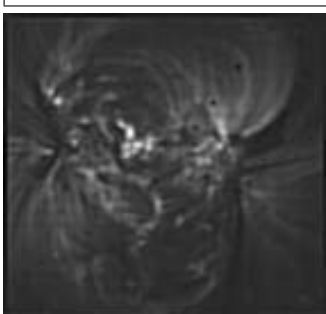
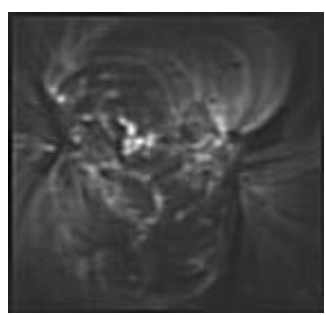
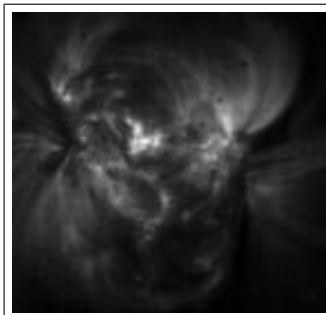
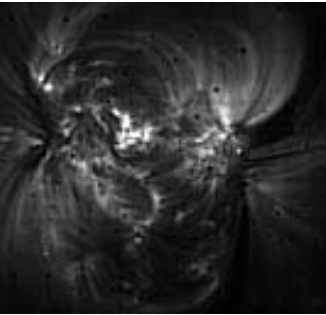
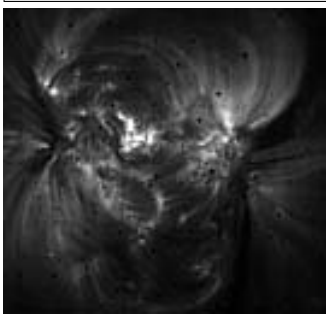
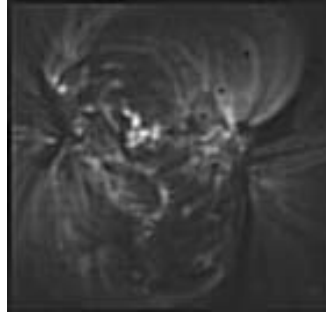
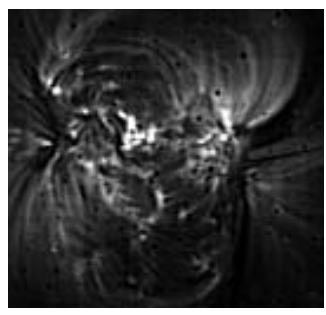
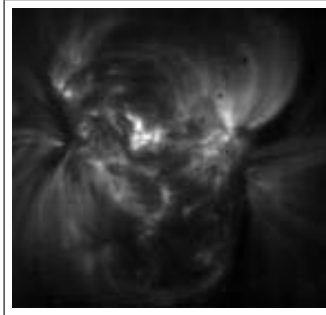


Fig. 13. Top foursome from left: Example of one input channel No. 4 (framed), and the VAM reconstructions from inputs No. 1, 2, 3 ; 4, 5, 6 ; 7, 8, 9. Bottom foursome from left: Example of one input channel No. 9 (framed), and the SAM reconstructions from the same inputs.

- [11] R. Chellappa and R. Kashyap, "Digital image restoration using spatial interaction models," *IEEE Trans. Acoustics, Speech and Sig. Proc.*, vol. 30, no. 3, pp. 284–295, June 1982.
- [12] S. Geman and D. Geman, "Stochastic relaxation , gibbs distributions and bayesian restoration of images," *IEEE Trans. Pattern Anal. Mach. Int.*, vol. 6, no. 11, pp. 721–741, November 1984.
- [13] D. Geman, *Random fields and inverse problems in imaging*. Berlin: Springer, 1990.
- [14] B. Jeffs and W. Pun, "Simple shape parameter estimation from blurred observations for a generalized gaussian mrf image prior used in map restoration," in *Proc. IEEE CVPR Conf.* San Francisco: IEEE, 1996,

Fig. 14. The SAM reconstruction result using nine input channels and its corresponding prediction probability (upper). Enlarged visualization of the model probability used to control restoration process - the 1st quadrant of adjacent image (bottom).

- pp. 465–468.
- [15] M. Stix, *The Sun*. Berlin, Heidelberg: Springer-Verlag Berlin Heidelberg New York, 2004.
- [16] B. Amizic, A. K. Katsaggelos, and R. Molina, "Using logarithmic opinion pooling techniques in bayesian blind multi-channel restoration," in *VISAPP (1)*, 2008, pp. 565–570.
- [17] F. Šroubek and J. Flusser, "Multichannel blind deconvolution of spatially misaligned images," *IEEE Trans. Image Processing*, vol. 14, no. 7, pp. 874–883, Jul. 2005.
- [18] M. Haindl, in *Proceedings of the 15th IAPR Int. Conf. on Pattern Recognition*, A. Sanfeliu, J. J. Villanueva, M. Vanrell, R. Alquezar, T. Huang, and J. Serra, Eds., vol. III. Los Alamitos: IEEE Press, September 2000, pp. 346–349.
- [19] R. Lagendijk, J. Biemond, and D. Boekee, "Identification and restoration of noisy blurred images using the expectation-maximization algorithm," *IEEE Trans. on Acoust., Speech, Signal Processing*, vol. 38, pp. 1180–1191, 1990.
- [20] M. Haindl and S. Šimberová, "Restoration of multitemporal short-exposure astronomical images," *Lecture Notes in Computer Science*, vol. 3540, pp. 1037–1046, June 2005.
- [21] F. Šroubek, G. Cristóbal, and J. Flusser, "A unified approach to super-resolution and multichannel blind deconvolution," *IEEE Trans. Image Processing*, vol. 16, no. 9, pp. 2322–2332, Sep. 2007.
- [22] V. Delouille, P. Chainais, and J.-F. Hochédez, "Spatial and temporal noise in solar EUV observations," *Solar Physics*, vol. 248/2, pp. 441–455, 2008.
- [23] M. Haindl and S. Šimberová, "Validation of classical and blind criteria for image quality evaluation," in *Proc. of the 9th IASTED Int. Conf. Signal and Image Processing*, R. de Figueiredo, Ed. Honolulu: ACTA Press, August 2007, pp. 218–223.